OKU Fen Bilimleri Enstitüsü Dergisi
9(4): 2354-2368, 2026

OKU Journal of The Institute of Science and Technology, 9(4): 2354-2368, 2026

Osmaniye Korkut Ata Üniversitesi
Fen Bilimleri Enstitüsü
Dergisi

Osmaniye Korkut Ata University
Journal of The Institute of Science
and Technology

K ve Ku Bant Uygulamaları için Dairesel Yama Mikroşerit Anten Tasarımı

Hemrah HIVEHCHI[1*]

[1]Lecturer, Department of Electrical – Vocational School, Istanbul Esenyurt University, Istanbul, Türkiye

[1]https://orcid.org/0000-0002-1708-5536

*Sorumlu yazar: hemrahhivehchi@esenyurt.edu.tr

Araştırma Makalesi

Makale Tarihçesi:
Geliş tarihi: 09.09.2025
Kabul tarihi:30.12.2025
Online Yayınlanma:09.09.2026

Anahtar Kelimeler:
Roger5880
Kusurlu toprak yapısı (DGS)
K-bant
Ku-bant

ÖZ

Bu çalışmada, K ve Ku bantlarında çalışacak şekilde dairesel bir mikroşerit yama anteni tasarlanmıştır. İstenilen frekans aralığı, kusurlu toprak yapısı (DGS) tekniği kullanılarak elde edilmiştir. Önerilen anten 30 × 35 × 0.8 mm3'lük kompakt bir boyuta sahiptir ve Rogers 5880 alt tabakasıyla simüle edilmiştir. Simülasyon sonuçları önerilen antenin geniş bant performansı gösterdiğini ve 12 GHz ile 22 GHz arasındaki frekans aralığını kapsadığını göstermektedir. Bant genişliği iyileştirmesi, yarım düzlem toprak yapısı kullanılarak elde edilmiştir. Anten parametreleri, uygun tasarım yöntemleri kullanılarak dikkatlice optimize edilmiştir.

Design of a Circular Patch Microstrip Antenna for K- and Ku-Bands Applications

Research Article

Article History:
Received: 09.09.2025
Accepted: 30.12.2025
Published online:09.09.2026

Keywords:
Roger5880
Defected ground structure (DGS)
K-band
Ku-band

ABSTRACT

In this work, a circular-shaped microstrip patch antenna is designed for operation in the K and Ku bands. The desired frequency range is achieved by employing the technique of Defected Ground Structure (DGS**)**. The proposed antenna has a compact size of 30 × 35 × 0.8 mm³ and is simulated with Rogers 5880 substrate. Simulation results show that the proposed antenna exhibits wide-band performance and covers the frequency range from 12 GHz to 22 GHz. Bandwidth enhancement is realized by incorporating a half-plane shaped ground structure. Antenna parameters are carefully optimized using appropriate design methods.

To Cite: Hivehchi H. Design of a Circular Patch Microstrip Antenna for K- and Ku-Bands Applications. Osmaniye Korkut Ata Üniversitesi Fen Bilimleri Enstitüsü Dergisi 2026; 9(4): 2354-2368.

1.Introduction

The continuous growth of wireless communication systems has driven substantial interest in the development of compact and wideband antenna structures. Among these, microstrip patch antennas stand out due to their lightweight form, ease of manufacturing, low profile and compatibility with integrated microwave circuits. These features make them highly suitable for modern broadband and high-data-rate applications, especially in systems requiring efficient spectrum utilization and compact integration. High data rates, improved spectral efficiency, and large bandwidth are essential to demands of wireless communication systems generation in future (Alsath and Kanagasabai, 2015). Microstrip slot antennas are considered promising candidates for Ultra-Wideband (UWB) applications due to their low profile, low cost, lightweight structure, and ease of integration with Monolithic Microwave Integrated Circuits (MMICs) (Karamzadeh and Mesut, 2014; Karamzadeh and Rafii, 2015).

In efforts to enable short-range, high-speed wireless connectivity, regulatory authorities have designated specific frequency bands for Ultra-Wideband (UWB) communication. Notably, in 2002, the FCC authorized the 3.1 GHz to 10.6 GHz range for UWB usage, targeting applications that demand high throughput over short distances. These include indoor wireless multimedia transmission, medical telemetry, and sensor networks operating with minimal interference to narrowband systems. Additionally, the X-band (8–12 GHz) and Ku-band (12–18 GHz), as defined by IEEE standards, are widely utilized in communication systems. The X-band finds applications in satellite communications, weather radar, defensive tracking, maritime vessel control, and speed detection systems. Similarly, the Ku-band is extensively used in fixed satellite services (FSS) and other satellite communication applications.

Several studies have explored innovative techniques to improve antenna bandwidth. In (Saha, 2019), a wideband response was achieved using a slotted circular patch along with a slotted ground structure. In (Suman, 2021), a novel bandwidth enhancement technique based on mode analysis was introduced, enabling a patch antenna to support more than three resonant modes. In (Devana, 2021), a flower-shaped antenna was proposed for UWB, C-band, X-band, and Ku-band applications, offering dual-band notch characteristics across 3.45 GHz to 18.5 GHz.

UWB technology is currently a focus of intense research due to its ability to deliver high-speed wireless interconnectivity for devices in close proximity. It supports the wireless transmission of video, audio, and high-bandwidth data over short distances (up to 10 meters), making it a preferred technology for eliminating cables in personal and professional device environments. UWB complements longer-range wireless technologies like Wi-Fi, WiMAX, and cellular networks by providing high-speed links over short distances (Rahayu, 2008).

The antenna presented in this work operates in the K and Ku bands and serves as a strong candidate for a wide range of applications, including radar systems, satellite communications, and 5G cellular networks**.** A comparison of performance with existing designs is provided in Table II**.**

This work presents the simulated of a microstrip patch antenna developed using a Rogers RT/Duroid 5880 substrate with a thickness of 0.8 mm. The antenna features a compact structure with overall dimensions of $30 \times 35 \times 0.8$ mm^3**.**

The radiating element consists of a circular patch with a semicircular slot, while the ground plane is designed in a half-plane rectangular shape, forming a Defected Ground Structure (DGS)**.** The introduction of DGS plays a crucial role in extending the antenna's operational range into the ultrawideband (UWB) spectrum (Guo and Min, 2019; Arnab, 2022). To further enhance the impedance bandwidth, a rectangular notch is etched into the ground plane—this modification is discussed in more detail in section 2 and 3**.**

2. Antenna Design Process

This section is organized into four parts, detailing the step-by-step design process of the proposed antenna. Throughout all design stages, the antennas are fabricated on a Rogers RT/Duroid 5880 substrate, which features a relative permittivity ε_r=2.2 and a loss tangent tanδ=0.0009. The feedlines are designed with a characteristic impedance of 50 Ω to ensure seamless integration with standard SMA connectors for measurement and testing (Balanis, 2005).

After than the rectangular patch, the next most widely used shape is the circular patch or disk. This structure has received significant attention not only as a single radiating element but also in array and broadband applications due to its compact size and symmetrical radiation characteristics. (Balanis., 2005).

In order to calculate the operating frequency of the circular patch antenna, the fundamental resonance mode TM_{11} must first be considered. The resonance frequency for this mode can be expressed as follows:

Resonance Frequency of Circular Patch Antenna presented as (Eq1): (Balanis, 2005):

Equation1:

$$f_r = \frac{F}{2\pi R\sqrt{\varepsilon_r}}$$

$$F = 1.8412C$$

f_r: Resonance frequency (Hz)

C: Speed of light 3×10^8 m/s

R: Radius of the circular patch (m)

ε_r: Relative permittivity of the substrate

1.8412: The first root of the derivative of the Bessel function (mod TM_{11})

F: dimensionless mode constant (F = 1.8412), while the speed of light, C, is an independent physical constant included in the formulation of the resonance frequency.

Circular microstrip antennas exhibit resonant behavior governed by electromagnetic boundary conditions, which are typically formulated using the Helmholtz equation in cylindrical coordinates. The solution of this equation leads to field distributions described by Bessel functions. For the dominant TM_{11} mode, resonance occurs at the first zero of the derivative of the Bessel function of the first kind, corresponding approximately to the value 1.8412. This root is fundamental in calculating the patch radius required for a desired operating frequency. The resulting field distributions are expressed in terms of Bessel functions, which naturally arise in the solution of the wave equation under circular symmetry.

The resonance frequencies of a circular patch antenna are determined by the zeros of the derivative of Bessel functions. Specifically, for the dominant TM_{11} mode, the resonance occurs when the first zero of the derivative of the Bessel function of the first kind J1′(x) is satisfied:

J1′(x)=0 The first root of this equation is approximately 1.8412, which is used in calculating the fundamental resonance frequency of the circular patch antenna. Jn′(x)=0 is used for the TM_{11} mode. The first root of this equation is approximately 1.8412. The value 1.8412 is the first root obtained for the fundamental resonance mode TM_{11} of the circular microstrip antenna, and it corresponds to the first zero of the derivative of the Bessel function. or more commonly presented as (Balanis, 2005):

$$f_r = \frac{1.8412C}{2\pi R\sqrt{\varepsilon_r}}$$

In this formula c is the speed of light in vacuum or free space, R is the radius of the circular patch, and ε_{eff} is the effective permittivity of the microstrip line which can be approximated as in (Eq.2) (Balanis, 2005).

Equation 2:

$$\varepsilon_{eff} = \frac{\varepsilon_r + 1}{2} + \frac{\varepsilon_r - 1}{2}\left(1 + \frac{10h}{R}\right)^{-1/2}$$

Here, ε_r is the relative electrical permittivity of the substrate and h is the substrate height. If we the effective permittivity is substituted into the formula for resonance frequency, the following can be obtained as in (Eq.3) (Balanis, 2005):

Equation 3:

$$f = \frac{C}{2\pi R\sqrt{\frac{\varepsilon r+1}{2}+\frac{\varepsilon r-1}{2}\left(1+\frac{10h}{R}\right)^{-1/2}}}$$

One can simply find the radius of the patch using the equation given below, as in (Eq.4) (Balanis, 2005):

Equation 4:

$$R= \frac{C}{2\pi f}\sqrt{\frac{\varepsilon_r+1}{2} + \frac{\varepsilon_r-1}{2}\left(1 + \frac{10h}{R}\right)^{-1/2}}$$

To ensure that the antenna operates at the desired resonance frequency, the radius of the circular patch must be appropriately calculated. Given that R represents the patch radius and h the substrate thickness, the effective radius can be determined based on the target resonance frequency and the relative dielectric constant of the substrate. This relationship is described by the following equation:

Eq. (5) (Balanis, 2005).

Equation5:

$$R= \frac{F}{\sqrt{1+\frac{2h}{\pi\varepsilon_r F}\left[\ln\left(\frac{\pi F}{2h}\right)+1.7726\right]}}$$

3. Antenna Design

The antenna design follows a stepwise refinement process:

3.1. Antenna I:

The initial simulated configuration of the proposed antenna is illustrated in Figure 1(a) (Hemrah and Karamzadeh, 2016; Sakshi and Jitesh, 2020). At this stage, the primary objective was to adjust the reflection-coefficient response to achieve an appropriate match with a 50 Ω feedline. At this stage, the primary objective was to adjust the impedance bandwidth to achieve an appropriate match with a 50 Ω feedline. The antenna I design and its performance analysis were conducted using ANSYS HFSS, version 16. For the preliminary design, the substrate dimensions were set to a width W=30 mm, L = 35 mm, and height h=0.8 mm. The simulation was initially performed using a simple circular patch placed centrally along the feedline, as shown in Figure 1. In this initial configuration the feed line length was set to $L_1 = 10.6$mm and the patch radius to $R = 8.5$mm." The simulated reflection coefficient S11 results corresponding to this configuration are shown in Figures 1(a) and (b). However, the initial S_{11} response did not meet the desired performance criteria, and Antenna I resonated only at 13.7 GHz with a minimum reflection coefficient of −16.95 dB thereby indicating the need for further optimization of the antenna I design.

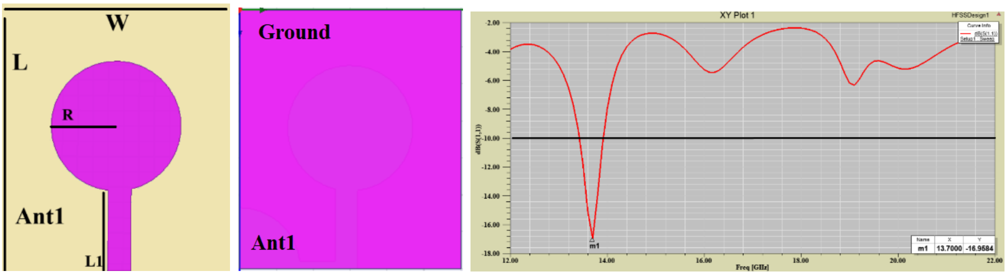

(a) (b)

Figure 1. (a) Configuration of the Antenna I (b) S11

3.2. Antenna II:

Based on our previous work and numerous studies in the literature on microstrip antennas, we decided to include a semicircular extension connected by a narrow strip within the patch, as shown in Figure 2. In this configuration, the semicircle radius was set to $R_c = 8.24$ mm, the strip width to $W_3 = 5$ mm, and the strip length to $L_4 = 1$ mm.

Following these design changes, a slight improvement in the S_{11} characteristic was observed at 13.7 GHz, where the reflection coefficient dropped to-21.65 dB. Therefore, we continued to refine the design by adding several grooves to the semicircular section to achieve further improvements, as shown in the last step (Karamzadeh and Hemrah, 2017; Ilkin et al. 2018)

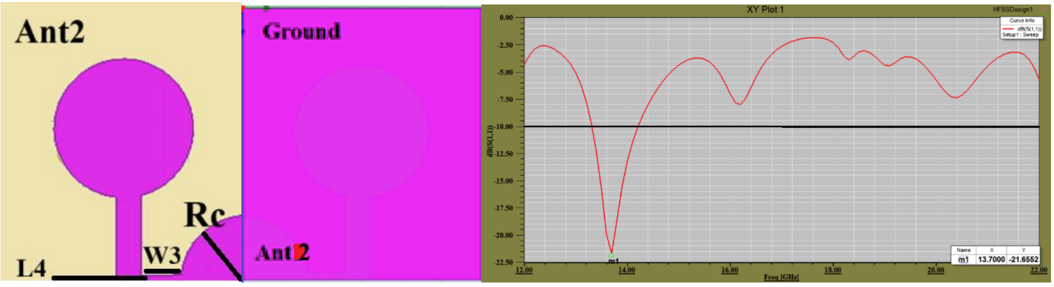

Figure 2. (a) Configuration of the antenna II (b) S11

3.3. Antenna III:

In the third stage of the design process, the reflection coefficient S11 was significantly improved by introducing gaps adjacent to the feedline and embedding five semicircular slots into the radiating patch. The configuration of this modified antenna III (referred to as Antenna II) and its corresponding simulation results are depicted in Figure 3 shows the antenna configuration. As shown in the S_{11} graph in Figure 3(b), the proposed antenna has an impedance bandwidth below -10 dB. The antenna resonates at 13.0 GHz, 18.1 GHz, 19.6 GHz and 20.6 GHz with corresponding reflection coefficients of -19.35 dB, -24.23 dB, -16.07 dB and -13.42 dB, respectively.

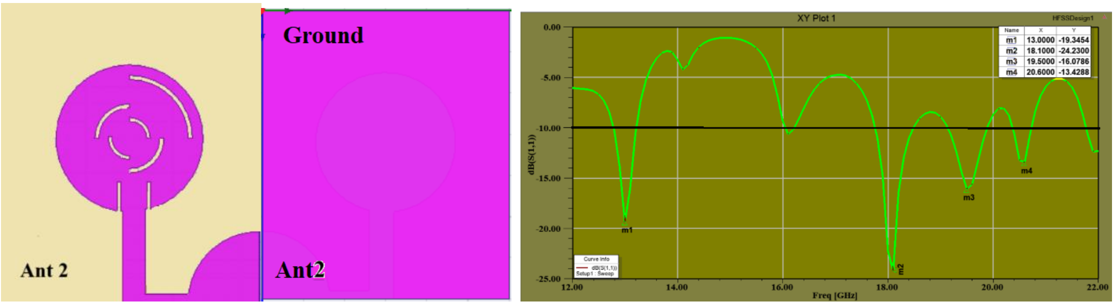

(a) (b)

Figure 3. (a) Antenna design III. Front view (Left side), back view (Right side), (b)S11

3.4. Antenna IV:

In the fourth design stage, The ground plane is truncated on both sides. These changes were implemented with the aim of further enhancing the reflection coefficient (S11) performance. The configuration of this revised antenna IV, Figure 4 presents the corresponding simulation results, where a strong resonance is observed at 16.9 GHz with an S_{11} magnitude of −32.14 dB.

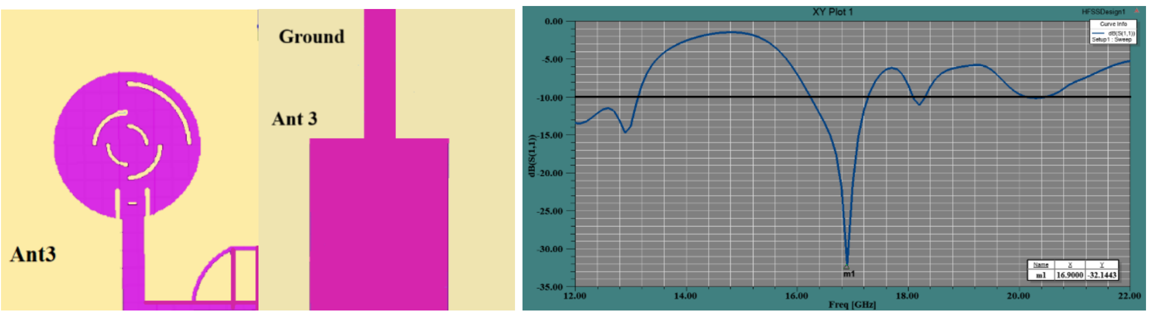

(a) (b)

Figure 4. (a)Antenna IV design. Front view (Left side), back view (Right side),(b)S11

3.5. Antenna V:

In the final design iteration, a rectangular shaped modification was incorporated into the ground plane, along with additional stepped features on both the ground and the radiating patch. These enhancements led to a notable improvement in the reflection coefficient (S11) performance. The configuration and simulation results of the optimized antenna V at this stage are shown in Figure 5. presents the complete single-element antenna V structure, including both front and back views, while the optimized design parameters are summarized in Table I.

A comprehensive review of recent literature indicates that the proposed antenna design demonstrates superior performance compared to many existing works, particularly in terms of impedance bandwidth, reflection coefficient (S11), and gain. In addition, the physical dimensions of the antenna have been significantly reduced relative to comparable designs, underscoring its compactness and suitability for space-constrained applications. A detailed comparative analysis between the proposed antenna V and previously reported designs is provided in Table II.

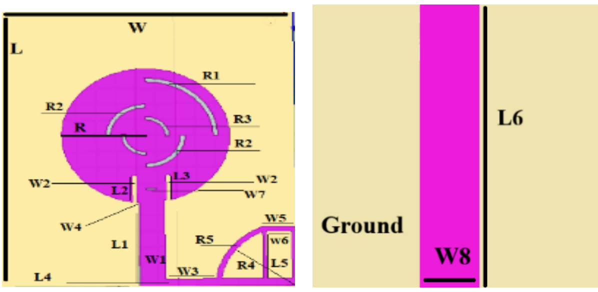

Figure 5. The designed antenna V with its detailed architecture

Table 1. Optimized dimensions

R=8.5	L=35	W=30
R1=0.4	L1=10.6	W1=2.56
R2=0.445	L2=3.38	W2=0.4
R3=0.407	L3=3.15	W3=5
R4=4.125	L4=1	W4=0.24
R5=0.628	L5=5.81	W5=3.5
-	L6=35	W6=2.5
-	-	W7=1*0.2
-	-	W8=4

4. Simulation Results

Figure 6 presents the S_{11} responses of all proposed antenna designs

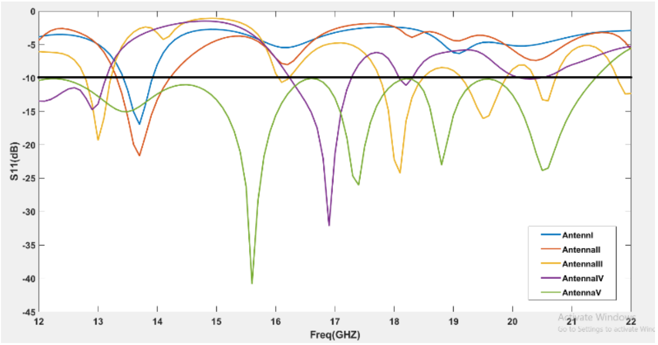

Figure 6. Simulated S11 for All antennas (I-V)

4.1. Reflection Coefficient (S11):

This section presents the reflection coefficient (S_{11}) as a function of frequency for the proposed antenna design. Figure 7 illustrates the S_{11} curves corresponding to each stage of the antenna development process.

In the final design (Antenna V)**,** The simulated results show that the proposed antenna V operates in a wide frequency range from 12 GHz to 22 GHz, and the reflection coefficient is kept below -10 dB in the entire band. It is noteworthy that this antenna V performs better at the frequencies of 15.6 GHz, 17.4 GHz, 18.8 GHz, and 20.5 GHz, where it has reflection coefficients reaching-40.83 dB,-20.03 dB, -23.03 dB, and -23.85 dB, respectively."

Highlighting the antenna's effectiveness in covering multiple frequency bands, including portions of the Ku, and K bands.

Additionally, a parametric analysis was carried out by varying key geometrical parameters to optimize the antenna performance. This helped in achieving the desired wideband response and improved impedance matching across the UWB range.

The parameter analysis performed to optimize the antenna performance is described in detail to quantitatively evaluate the contribution of each design variable to the electromagnetic behavior of the structure. The results show that the operating bandwidth has a strong correlation with the parameters that modify the effective radiation aperture and resonance modes, such as patch radius, length-to-width ratio of the DGS slot, and substrate thickness. In contrast, the input impedance matched to the 50-ohm feedline is primarily controlled by the feedline width, the optimized feedpoint offset in the x-z plane, and the slot geometry, which together modify the local surface current distribution. The influence of each parameter on the S11 characteristics is simulated separately, and the corresponding changes in resonance depth, impedance slope, and equivalent loading effects are analyzed to guide the final design optimization.

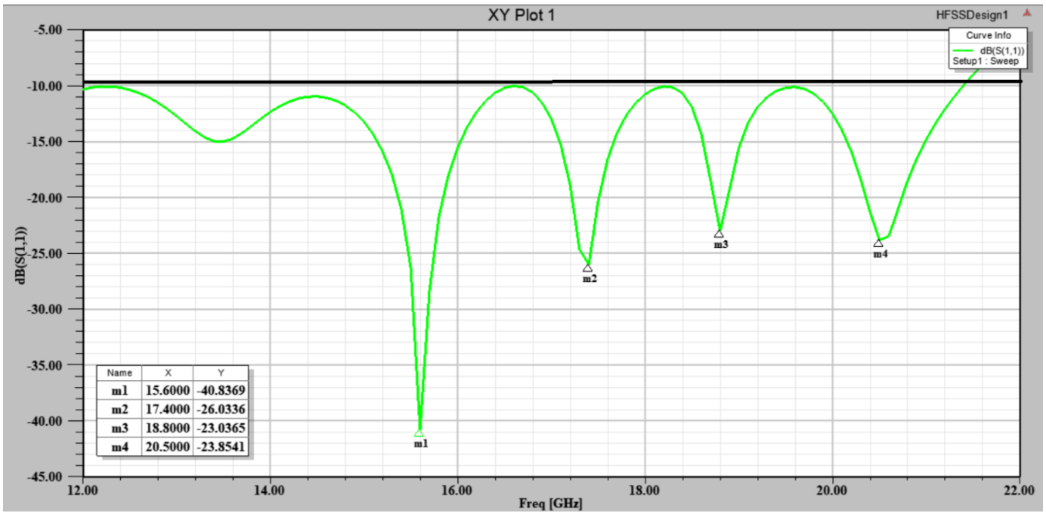

Figure 7. Reflection coefficient (S_{11}) curve plot showing the stepwise development of antenna V.

4.2. Gain, PeakGain and Radiation Pattern:

This antenna V covers a range of wide frequency which inherently affects its gain characteristics. Despite the modest gain levels, the antenna V offers a good trade-off between compact size, low cost, and wide bandwidth, making it a suitable candidate for wireless communication applications (Balanis, 2005).

As illustrated in Figure 8, the gain values at the frequencies 15.6 GHz, 17.4 GHz, 18.8 GHz, 20.5 GHz are 0.15, 0.86, 1.22 and 1.11, respectively. These values indicate excellent impedance matching across the operating band. The corresponding gain values at the evaluated frequencies are 5.37dBi, 4.28dBi, -0.11dBi, -0.39dBi, and 4.98dBi. At 12.2 GHz, the antenna V exhibits weak radiation with a gain of -0.11dBi. The antenna V exhibits strong radiation performance at 15.6, 17.4, and 20.5 GHz, while at 18.8 GHz, the gain drops to -0.39dBi, indicating poor radiation efficiency.

After simulating the proposed antenna V, its peak gain across the operating frequency band was evaluated. As shown in Figure 9, the antenna's maximum peak gain was 7.198 dBi at 19.80 GHz. At other key frequencies in this band, the antenna exhibited peak gains of 5.83 dBi at 15.6 GHz, 5.27 dBi at 17.4 GHz, 6.21 dBi at 18.8 GHz, and 5.69 dBi at 20.5 GHz. These results demonstrate that the antenna V maintains a relatively high gain across the desired frequency range, demonstrating its effectiveness for applications requiring moderate directional performance.

The simulated radiation patterns of the final antenna design are depicted in Figure 10.

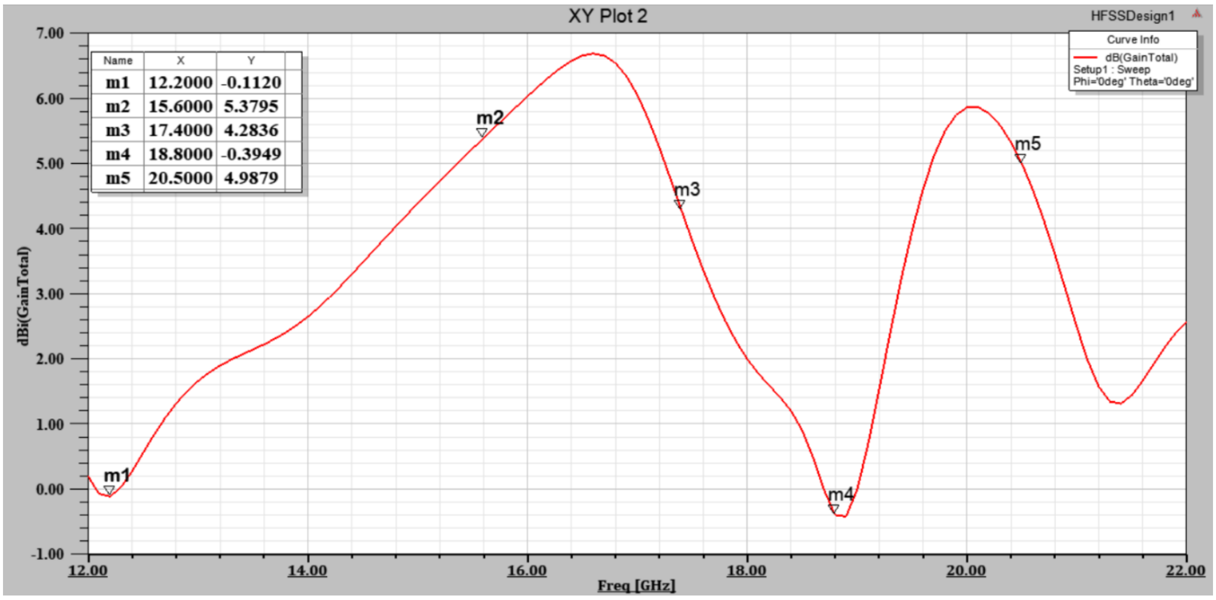

Figure 8. The Gain of antennaV

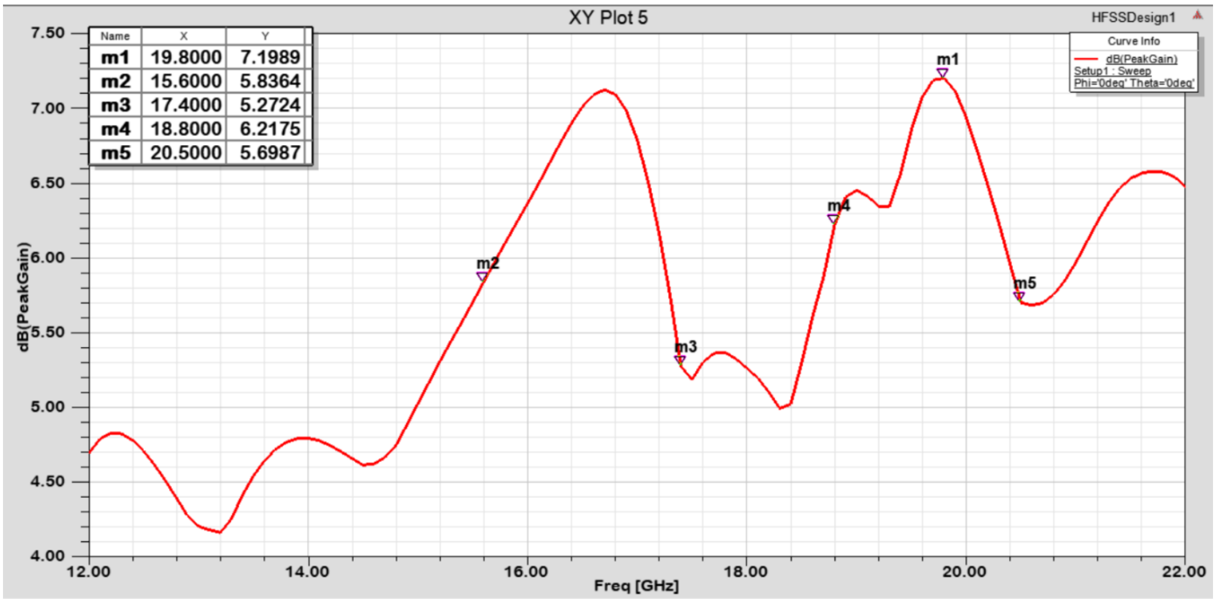

Figure 9. The Peak Gain of antennaV

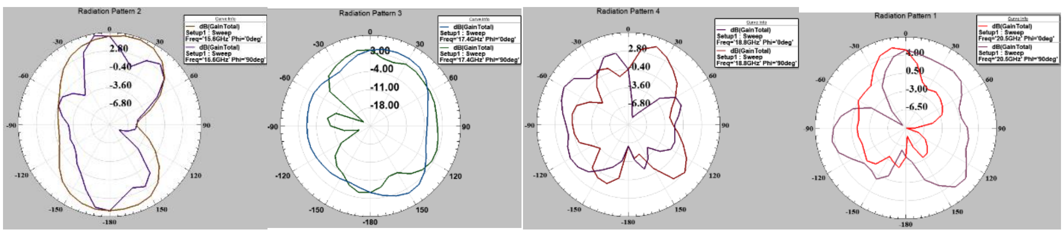

a) b) c) d) e)

Figure 10. Simulated radiation patterns of the designed antennaV at (a) 15.6 GHz (b) 17.4 GHz (c) 18.8 GHz (d) 20.5 GHz

4.4. VSWR:

When the transmission line of antenna is connected to antennaV systems as is typically the case impedance matching can be accomplished by end of the line. However, in practical applications, the matching is usually implemented near the antenna V terminals, as this approach minimizes line losses, reduces voltage standing waves along the transmission line, and helps maximize the system's usable bandwidth (Balanis, 2005).

In a mismatched system, the degree of mismatch determines the portion of incident (or available) power that is reflected back into the transmission line from the antennaV input. This mismatch arises from the difference between the antenna input impedance and the characteristic impedance of the transmission line (Balanis, 2005).

These quantities are related to the input reflection coefficient (GammaΓ) and the Voltage Standing Wave Ratio (VSWR) at the antennaV terminals. The standard transmission line relationships are given by (Balanis, 2005).

$$\Gamma = \frac{Z_{in} - Z_0}{Z_{in} + Z_0}$$

$$VSWR = \frac{1+|\Gamma|}{1-|\Gamma|}$$

where:

- Zin input impedance of antenna,
- Z0 is the characteristic impedance of the transmission line,
- Γ GammaΓ is the reflection coefficient.

These expressions are essential for evaluating the impedance match quality and the overall efficiency of the antenna-feed system. (Balanis, 2005). Figure 11 illustrates the simulated Voltage Standing Wave Ratio (VSWR) performance of the proposed antenna at key resonant frequencies. The VSWR values at 15.6 GHz, 17.4 GHz, 18.8 GHz, and 20.5 GHz are 1.018, 1.105, 1.151, and 1.137, respectively. All values remain well below the standard threshold of 2.

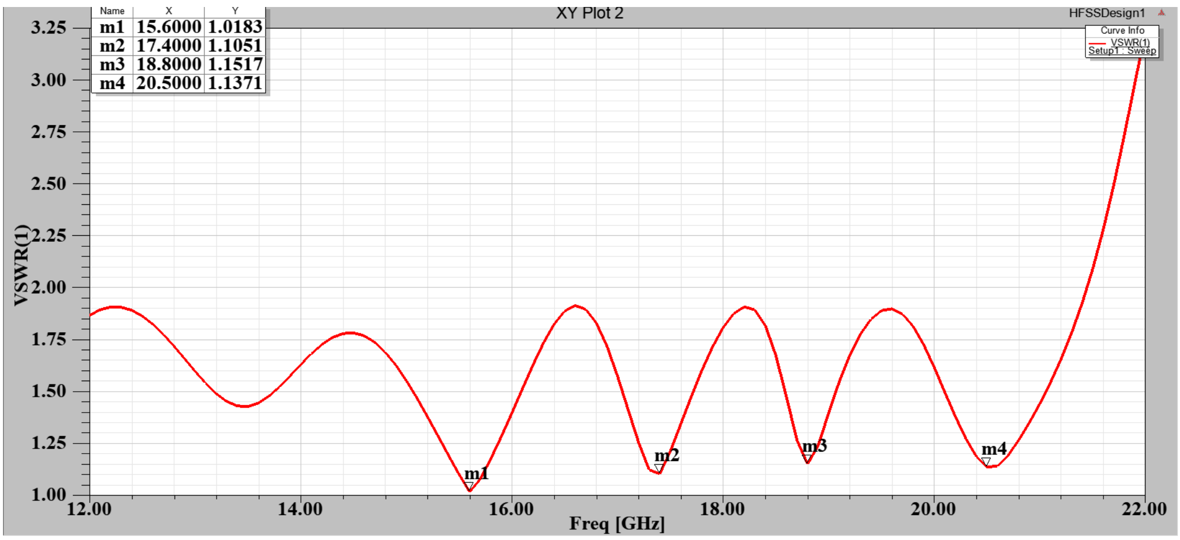

Figure 11.VSWR of antenna

5. Comparative Analysis

Compared to existing designs, the proposed antennaV supports broader bandwidth while maintaining a small footprint. Unlike many dual-band or tri-band antennas, this design simultaneously supports operation in X-, K-, and Ka-bands with superior return loss and gain.

Moreover, while several designs have been proposed for specific 5G frequency bands, this antenna is distinctly optimized to cover the critical 8 GHz and 22 GHz frequencies. The consistently low reflection coefficients and high gain across all resonant bands underscore the superior performance and practicality of the proposed antennaV for compact, high-efficiency wireless systems.

Table 2. Comparison with other works

Reference	Substrate/ Thickness (mm)	Size (mm^2)	Operating Frequency Range (GHz)	Maximum Peak Gain (dB)
Kiruthika, 2018	FR4/1.6	31 x 28	7-13	3.3
Singh,2019	FR4/1.6	25 x 25	4-8	-
Sakshi Singh12020	FR4/2	14.3 x14.3	9.528, 12.806, 19.173	-
Singh,2020	FR4/0.7	50 x 50	2-7	6.99
Suman Sharma,2021	FR4/1.56	40×40	9.6,13.6	5.88
Hossain,2022	FR4/0.5	20×60	9.03,10.12,14.3	4.13
Lavadiya, Sunil P2022	FR4/1.5	31 x 42	2-16	2.27
Madhusudhana, K2022	FR4/1.6	41 x 41	1-6	-
Muhammad Danny2024	Rogers 5880/1.6	15×40	9-10, 13,5-14,5	5.29
Ananda Kumar2024	FR4/1.6	10 × 10	10.58–15.04	5.675
Proposed Antenna	Roger5880/0.8	30×35	12-22	7.19

6. Conclusion

This study demonstrates the effectiveness of the proposed microstrip patch antennaV for K- and Ku-band applications (12–22 GHz), achieving notable improvements in gain, bandwidth. The integration of a Defected Ground Structure (DGS) and optimized slot geometries has contributed to enhanced wideband performance, rendering the antennaV well-suited for high-frequency applications.

Despite these advancements, the design presents certain limitations in maintaining consistent performance across the entire targeted bandwidth. This highlights the need for further optimization of slot dimensions and their spatial configuration. Future research may focus on refining structural parameters and investigating alternative feeding techniques to improve overall efficiency and ensure uniform bandwidth coverage.

With its compact size and strong performance characteristics, the proposed antenna exhibits significant potential for deployment in advanced satellite communication systems, radar technologies, and emerging 5G and beyond wireless networks.

References

Alsath GN., Kanagasabai M. Compact uwb monopole antenna for automotive communications. IEEE Transactions on Antennas and Propagation 2015: 63(9): 4204-4208.

Arnab D., Roy B., Bhattacharya A., Bhattacharjee AK. Investigations on a circular uwb antenna with archimedean spiral slot for wlan/wimax and satellite x-band filtering feature. International Journal of Microwave and Wireless Technologies 2022: 781-789.

Balanis CA. Antenna theory analysis and design. 3rd Ed., John Wiley, Sons, New Jersey, 2005.

Behera A K., Konhar D., Tripathy SH. X-sphere pillar patch antenna For x- ku-band operation. 2nd International Conference on Signal Processing, Communication, Power and Embedded System (SCOPES) 2024: 979-8-3315-0645.

Chen C. A Uniplanar ultrawideband antenna with unidirectional radiation for wlan/wimax applications in IEEE Antennas and Wireless Propagation Letters 2021:743-747.

Devana VKNR., Rao AM. A compact flower slotted dual band notched ultrawideband antenna integrated with ku band for ultrawideband, medical, direct broadcast service, and fixed satellite service applications. Microw Opt Technol Lett 2021; 63: 556–563.

First report and order on ultra-wideband technology. FCC, Washington, DC, USA.

Ghosh A., Mandal T., Das S. Design and analysis of triple notch ultrawideband antenna using single slotted electromagnetic bandgap inspired structure. Journal of Electromagnetic Waves and Applications 2019: 1391-1405.

Guo L., Min M., Che W., Yang W. A novel miniaturized planar ultra-wideband antenna in IEEE Access 2019: 2769-2773.

Hammache B., Messai A., Messaoudene I., Denidni TA. A compact ultrawideband antenna with three c-shaped slots for notched band characteristics. Microwave and Optical Technical Letter 2019; 61: 275–279.

Hemrah H., Karamzadeh S. New Compact Circular Polarized CPW Antenna Design for UWB Application.International Journal Of Electronics, Mechanical And Mechatronics Engineering 2016 :1433-1439.

Hossain S., Rafiq G., Md. Roknuzzaman K. Design and analysis of Triple band microstrip antenna using slotted patch for x and ku-band application. 1st International Conference on Computational Science and Technology 2022.

Ilkin I., Hemrah H., Karamzadeh S. A New Triple Band Antenna Design for GPS/ WLAN/ WIMAX Applications. International Journal Of Electronics, Mechanical And Mechatronics Engineering 2018: 1505-1513

Karamzadeh S., Hemrah H. A new CPW-fed circularly polarized square slot antenna design. IU-JEEE 2017: 3141-3145

Karamzadeh S., Kartal M., Kent S., Ashtiyani AA. Optimal signal processing method in uwb radar for hidden human detection. 10th European Conference on Synthetic Aperture Radar EUSAR 2014.

Karamzadeh S., Rafii V., Kartal M., Saygin H. Compact UWB cp square slot antenna with two corners connected by a strip line. Electronics Letters 2015.

Kiruthika R., Shanmuganantham T. Design and measurement of novel shaped microstrip antenna with dgs for radar applications. International Journal of Wireless and Microwave Technologies 2018.

Liu J. A low-profile directional ultrawideband antenna. in IEEE Antennas and Wireless Propagation Letters 2018: 255-259.

Lavadiya s., Sunil P., Sorathiya V., Kanzariya S., Chavda BH. Low profile multiband microstrip patch antenna with frequency reconfigurable feature using pin diode for s, c, x, and ku band applications. International Journal of Communication Systems 2022.

Midya M., Bhattacharjee S., Mitra M. Circularly polarized planar monopole antenna for ultra wideband applications. International Journal of RF and Microwave Computer-Aided Engineering 2019.

Madhusudhana K., Shriram P., Hegde. Reconfigurable fractal microstrip antenna with varactor diode. Global Transitions Proceedings 2022.

Peddakrishna S., Khan T. Design of uwb monopole antenna with dual notched band characteristics by using π-shaped slot and ebg resonator. Aeu-International Journal of Electronics and Communications 2018; 96: 107–112.

Shakib MN., Moghavvemi M., Mahadi WNL. A low-profile patch antenna for ultrawideband application.in IEEE Antennas and Wireless Propagation Letters 2015: 1790-1793.

Sakshi S., Jitesh K. Miniaturized triband circular patch antenna for X Band, Ku Band and K Band applications. 9th International Conference System Modeling and Advancement in Research Trends (SMART) 2020: 978-1-7281-8908-6

Singh R., Pujara DA. A novel design of ultra-wideband quarter circular microstrip monopole antenna. Microwave and Optical Technical Letter 2017; 59: 225-229.

Singh PP., Sharma SK., Kalia P., Goswami PK. A frequency reconfigurable circular microstrip patch antenna using pin diode. 8th International Conference System Modeling and Advancement in Research Trends 2019.

Saha TK., Goodbody C., Karacolak T., Sekhar PK. A compact monopole antenna for ultra-wideband applications. Microwave and Optical Technical Letter 2019: 61:182–186.

Singh S., Kumar J. Miniaturized triband circular patch antenna for x band, ku band and k band applications. 9th International Conference System Modeling and Advancement in Research Trends 2020: 978-1-7281-8908-6.

Sharma S., Kumar M., Nigam H., Mathur M. Dual band circular patch coplaner microstrip patch antenna for x band and ku band applications. IEEE Indian Conference on Antennas and Propagation 2021: 978-1-6654-0110-4.

Singh RK., Basu A., Koul SK. Reconfigurable microstrip patch antenna with polarization switching in three switchable frequency bands. in IEEE Access 2022: 119376-119386.

Syach MDN., Wahdiyat AM., Apriono C. Enhanced triple-slot microstrip patch antenna for superior bandwidth and performance in x-band and ku-band systems. 7th International Seminar on Research of Information Technology and Intelligent Systems 2024: 979-8-3315-1964-3.

Yang H., Xi X., Zhao Y., Wang L., Shi X. Design of compact ultrawideband slot antenna with improved band-edge selectivity. in IEEE Antennas and Wireless Propagation Letters 2018: 946-950.